Supplementary Information

Quantifying buffer transport–limited water electrolysis at non-extreme pH by numerical simulation

*Melody Wada, Keisuke Obata, Kazuhiro Takanabe**

Department of Chemical System Engineering, School of Engineering, The University of Tokyo,

7-3-1 Hongo, Bunkyo-ku, Tokyo, 113-8656, Japan

Figure S1-S16
Table S1-S6

1. Experimental behavior

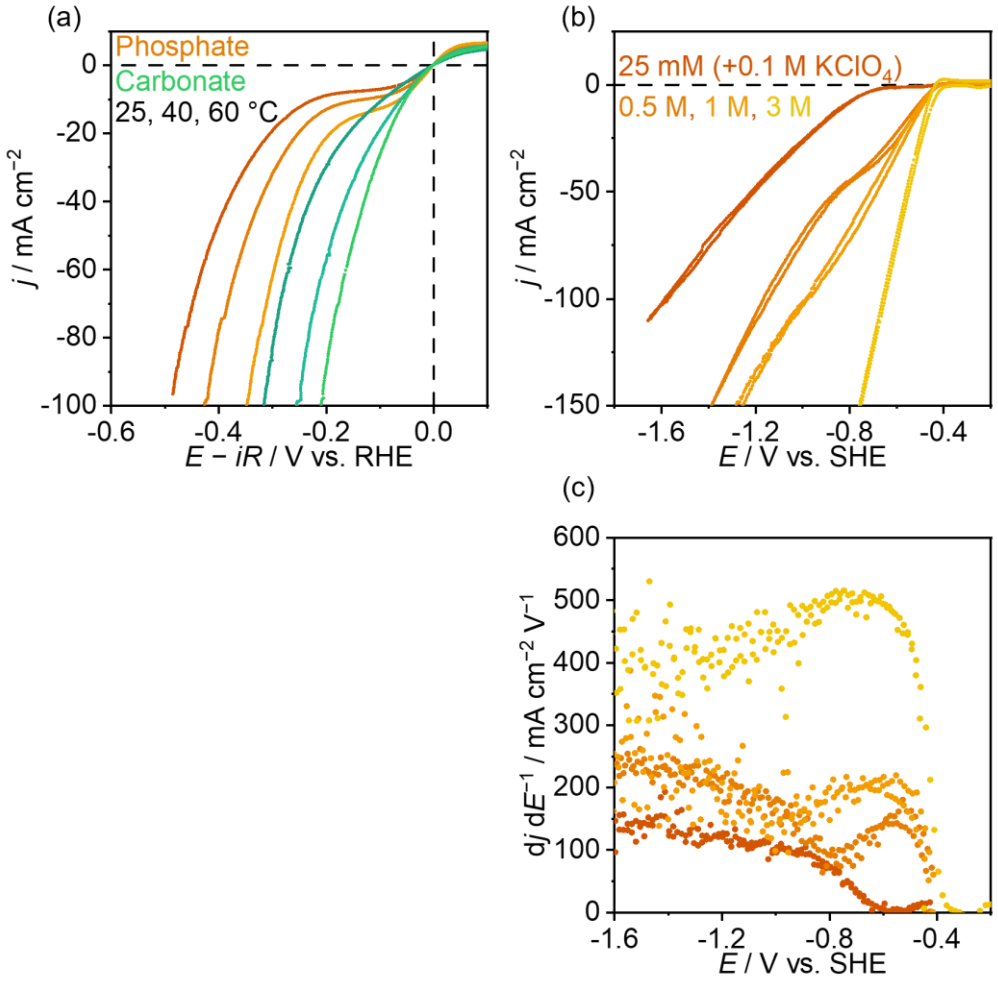

Fig. S1 (a) Experimentally measured cyclic voltammograms at various temperatures with a scan speed of 200 mV s^{-1}. Electrolyte pHs were adjusted to near 7.2 or 10.3 at room temperature for K-phosphate and K-carbonate, respectively. The Pt rotating disk electrode was rotated at 4,900 rpm. Supporting salt (0.1 M $KClO_4$) was added in 25 mM buffer electrolyte at room temperature. (b) Experimentally measured cyclic voltammograms with Pt foil for various concentrations of K-phosphate buffer solutions at room temperature with a scan rate of 200 mV s^{-1}. The pH of all electrolytes was adjusted to approximately 7.2. (c) Differentiation of current density as a function of potential using the data of (b).

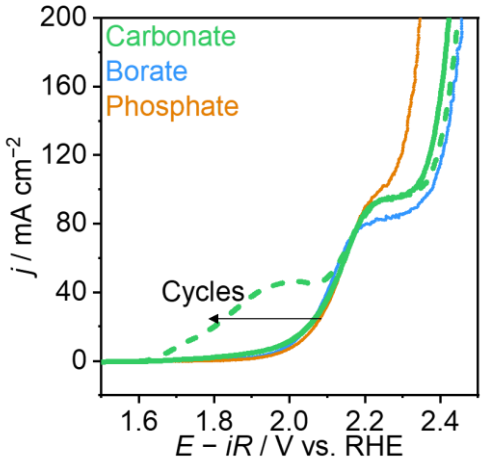

Fig. S2 Experimentally measured cyclic voltammograms with a scan speed of 200 mV s^{-1} under O_2 flow. The electrolyte pH was adjusted to near 10.3, 9.2 or 7.2 at room temperature for Na-carbonate, Na-borate or Na-phosphate, respectively. A Ni rotating disk electrode was rotated at 4900 rpm. Supporting salt (1 M $NaClO_4$) was added in all electrolytes. Green line shows the first cycle in carbonate and dash line shows cycle 12.

2. Model details

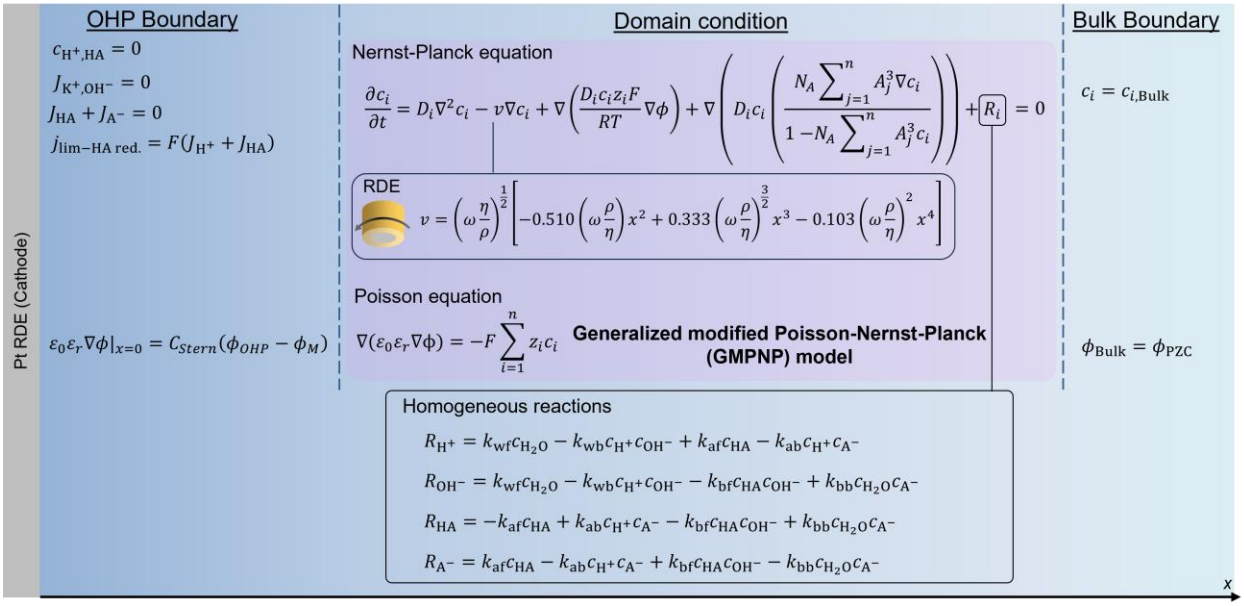

Fig. S3 Illustration of the model to simulate the limiting current density of direct buffer reduction during the HER, $j_{\text{lim-HA red.}}$, which was investigated by focusing on the flux of protonated buffer species at the electrode surface.

Crowding effect with different ion sizes

The steric term, J_{Steric}, is phenomenologically added to the equation of flux to explain crowding effects at the electrical double layer, EDL, caused by the finite ion sizes.[52] Many studies in this field use the following expression:[33-35]

$$J_{\text{Steric}} = -D_i c_i \nabla\left(\ln\frac{1}{1 - \sum_{i=1}^{n}\frac{c_i}{c_{i,\,max}}}\right) \tag{S1}$$

where $c_{i,\text{max}}$ represents the maximum ion concentration determined by $c_{i,\text{max}} = 1/(N_A A_i^3)$. N_A is the Avogadro's number and A_i is the size of species i. As ion concentration increases, the value of $1 - \sum_{i=1}^{n}\frac{c_i}{c_{i,\,max}}$ approaches 0. When solvated ion sizes are applied as A_i, it reaches 0 above 1.5 M of K-buffer solutions, which is physically unrealistic. This steric expression assumes that all ions exist independently with being fully covered by water, which is not applicable in concentrated electrolytes where water surrounding ions can be replaced by other ions or shared by several ions. These situations can be assumed whether the actual ions are smaller than fully water

surrounding ions or actual concentrations of species are smaller. Therefore, our model used thermochemical ion sizes, which can be the minimum ion size.

Next, how ion sizes influence the simulated results of limiting current of direct buffer reduction, $j_{\text{lim-HA red.}}$ was investigated. Fig. S4 shows a comparison of $j_{\text{lim-HA red.}}$ with different ion sizes in 3 M K-buffer electrolyte. The electrolyte pH was assumed to match the pK_a of the buffer. Ion sizes were considered 0 without the crowding effect. While ion sizes did not affect the value in phosphate, they changed that in carbonate. Fig. S5 and S6 summarize concentration profiles of ions in phosphate and carbonate, respectively. In both electrolytes, K^+ concentration at EDL decreases as ion sizes increase because ions with large size pack large area and suppress ions' crowding. Accordingly, the other ion concentrations also change at EDL. In phosphate, however, the concentration profiles in diffusion layer are not affected by ion sizes. On the other hand, profiles in carbonate show different behavior according to ion sizes. As discussed in main text, $j_{\text{lim-HA red.}}$ in buffer electrolytes with small pK_a is determined by diffusion from the bulk. In buffer electrolytes with large pK_a, buffer concentration profile at EDL affects $j_{\text{lim-HA red.}}$ significantly.

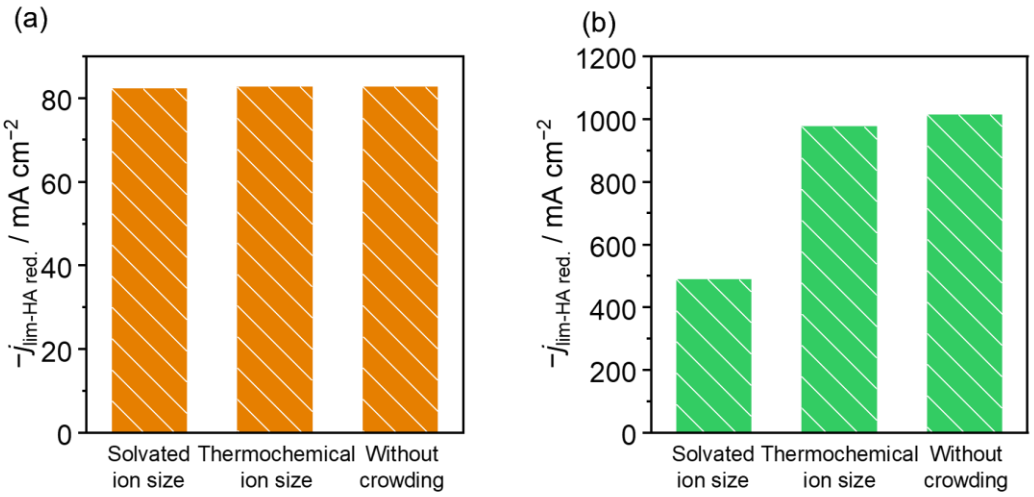

Fig. S4 Calculated limiting current density of direct buffer reduction, $j_{\text{lim-HA red.}}$ considering different ion sizes. Without crowding was calculated assuming ion diameter is 0. We assumed 1.5 M K-buffer, meaning pH value was its pK_a value. Pt rotating disk electrode was assumed to rotate at 100 rpm at 25 °C. (a) K-phosphate at pH 7.2. (b) K-carbonate at pH 10.3.

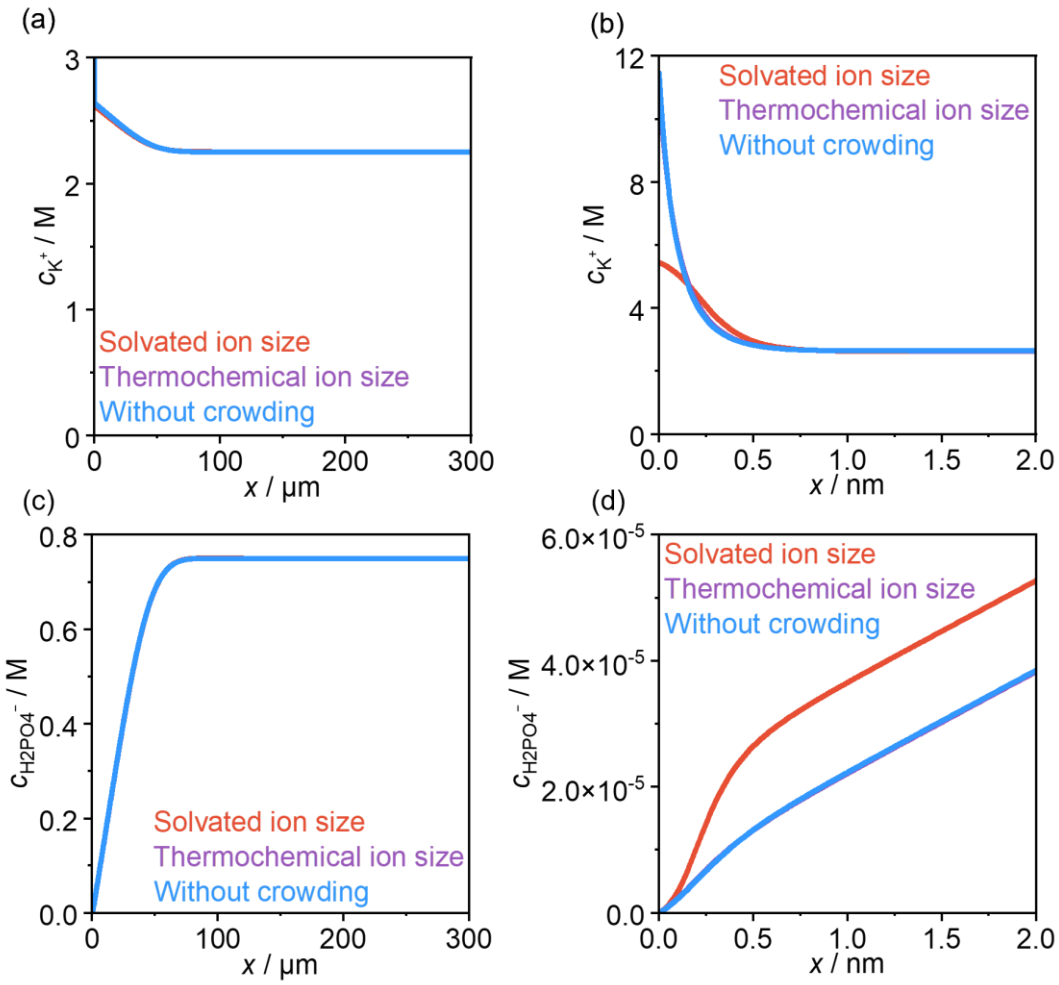

Fig. S5 The simulated ion concentration profiles in the solutions as a function of distance from the electrode surface in 1.5 M K-phosphate at pH 7.2. Pt rotating disk electrode was assumed to rotate at 100 rpm at 25 °C. (a,b) K^+ profile at different range. (c,d) $H_2PO_4^-$ profile at different range.

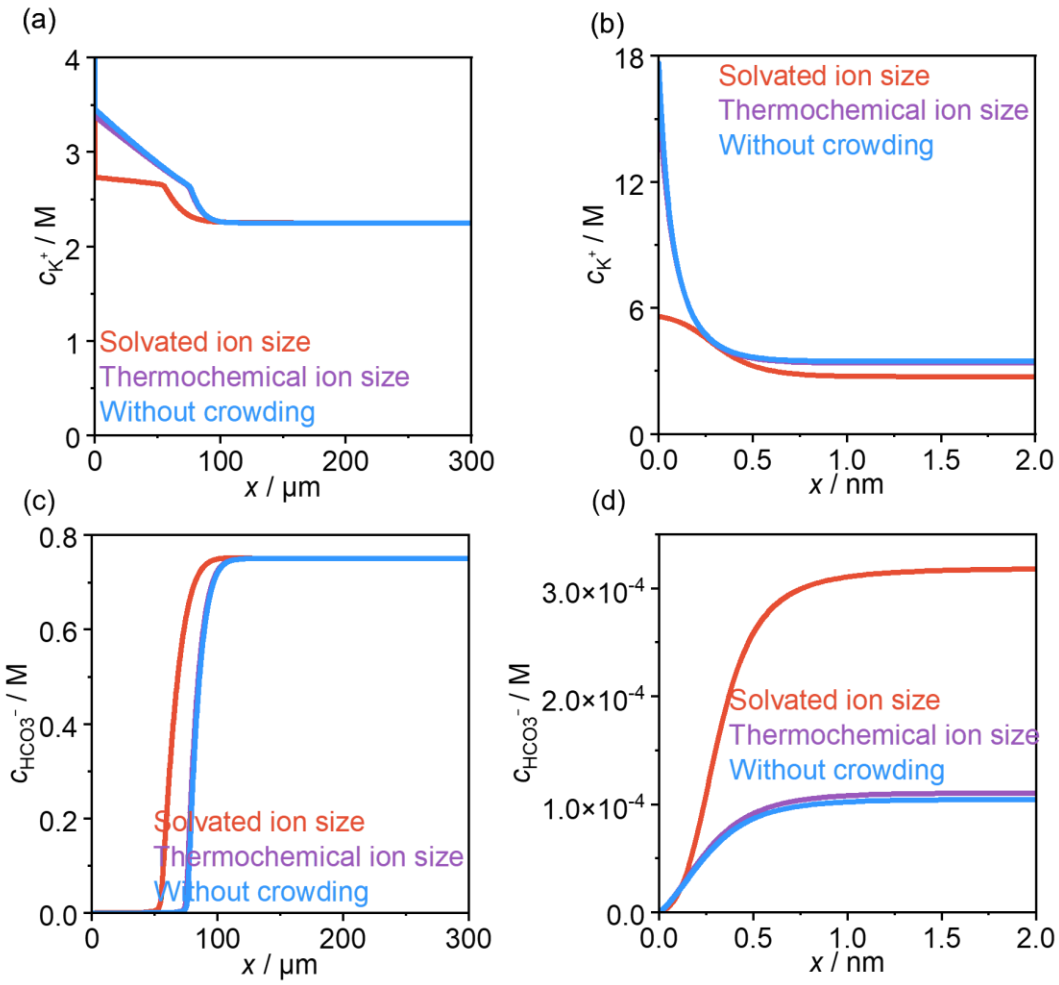

Fig. S6 The simulated ion concentration profiles in the solutions as a function of distance from the electrode surface in 1.5 M K-carbonate at pH 10.3. Pt rotating disk electrode was assumed to rotate at 100 rpm at 25 °C. (a,b) K^+ profile at different range. (c,d) HCO_3^- profile at different range.

Activity and concentration

To model the mass transport of species, we employed concentration instead of activity even though our previous work suggested that using activity provides an accurate representation for concentrated solutions.[15] The equation for material balance (Eq. 9) remains valid for all types of solution. However, in concentrated solutions, species interaction must be considered, which results in mutual dependence of concentration gradients of species.[53] For simplicity, our model assumes that these interactions are negligible, allowing the flux to be expressed in terms of electrochemical potential μ_i:

$$J_i = -M_i c_i \nabla \mu_i + c_i v \tag{S2}$$

where M_i represents the mobility of species i. The electrochemical potential is the sum of the chemical potential and the electrical potential of the species given by:

$$\mu_i = k_B T \ln a_i + z_i e\phi \tag{S3}$$

The corresponding flux equation is:

$$J_i = -\frac{M_i c_i}{k_B T}\nabla\left(\ln \gamma_i + \ln c_i\right) - M_i c_i z_i e\nabla\phi + c_i v = -\frac{M_i}{k_B T}\left(c_i \nabla \ln \gamma_i + \nabla c_i\right) - M_i c_i z_i e\nabla\phi + c_i v \tag{S4}$$

Under the assumption of a dilute solution (γ_i = 1) or unity for activity coefficients throughout the domain, this simplifies to:

$$J_i = -\frac{M_i}{k_B T}\nabla c_i - M_i c_i z_i e\nabla\phi + c_i v \tag{S5}$$

Therefore, using concentration for the flux of species is more reasonable. Of note, this is the Nernst-Planck equation and a previous study applied to 3 M $KHCO_3$ electrolyte.[54] In terms of activity coefficients, the flux of species depends on the spatial gradient of the activity coefficient, rather than on the value itself. Activity coefficients are affected by the ionic strength. As shown in Fig. S5, the ionic strength in phosphate electrolyte slightly increases at diffusion layer (−60 μm), while the significant increase occurs at EDL. As discussed, $j_{\text{lim-HA red.}}$ in buffer electrolytes with small pK_a is caused by diffusion from the bulk, implying the spatial gradient of the activity coefficient at EDL is not likely influential. On the other hand, buffer concentration profile at EDL affects $j_{\text{lim-HA red.}}$ in buffer electrolytes with large pK_a, which may indicate the spatial gradient of the activity coefficient at EDL changes $j_{\text{lim-HA red.}}$. However, it is difficult to apply the model for activity coefficients, such as Pitzer equation, which determines the activity coefficient of species in the bulk solutions while the strong electric field and non-uniform ion distribution exist at EDL. Therefore, this study ignored the spatial gradient of the activity coefficient. Instead, the GMPNP model incorporates additional terms to account for the crowding effects, which inhibit the unrealistic high concentration at the surface.

3. Data in phosphate and carbonate electrolytes

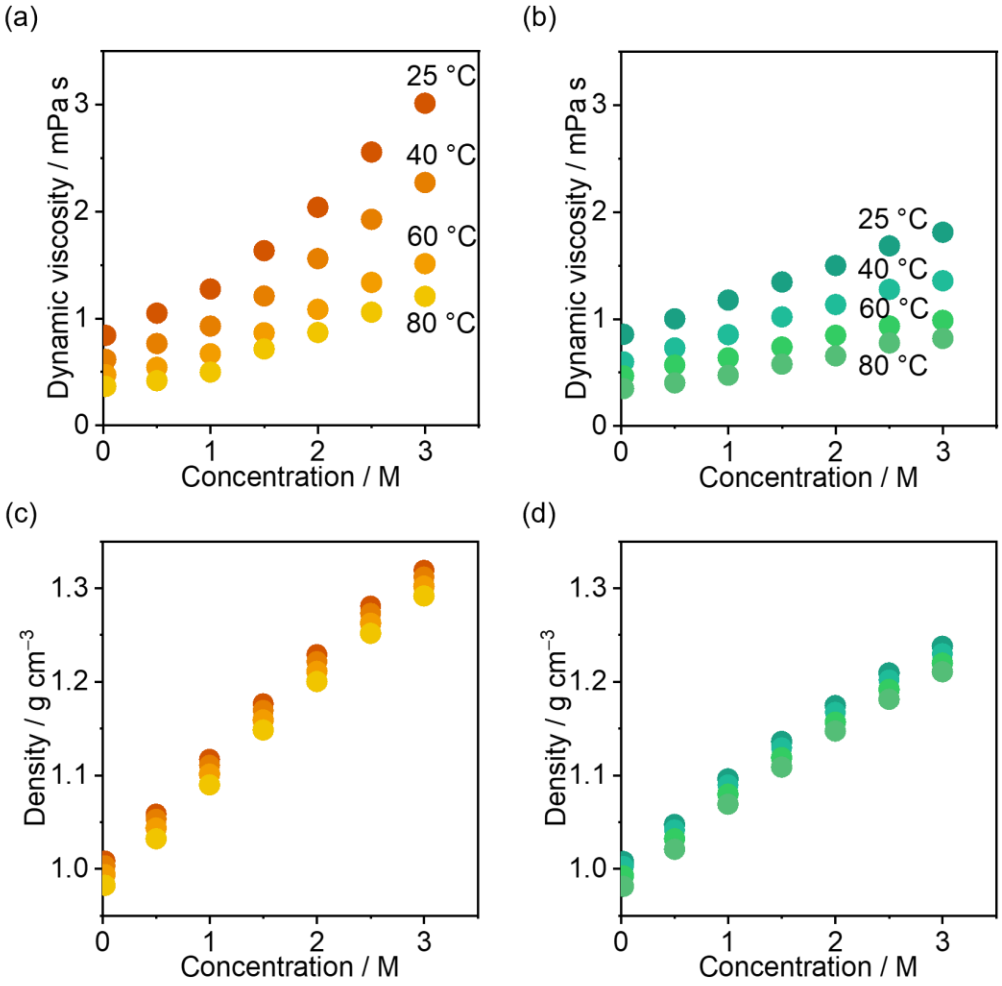

Fig. S7 (a) Experimentally measured dynamic viscosity of K-phosphate. Electrolyte pHs were adjusted to near 7.2 at room temperature. (b) Dynamic viscosity of K-carbonate. Electrolyte pHs were adjusted to near 10.3 at room temperature. (c) Density of K-phosphate. (d) Density of K-carbonate. Supporting salt of 0.1 M $KClO_4$ was added in 25 mM buffer electrolyte.

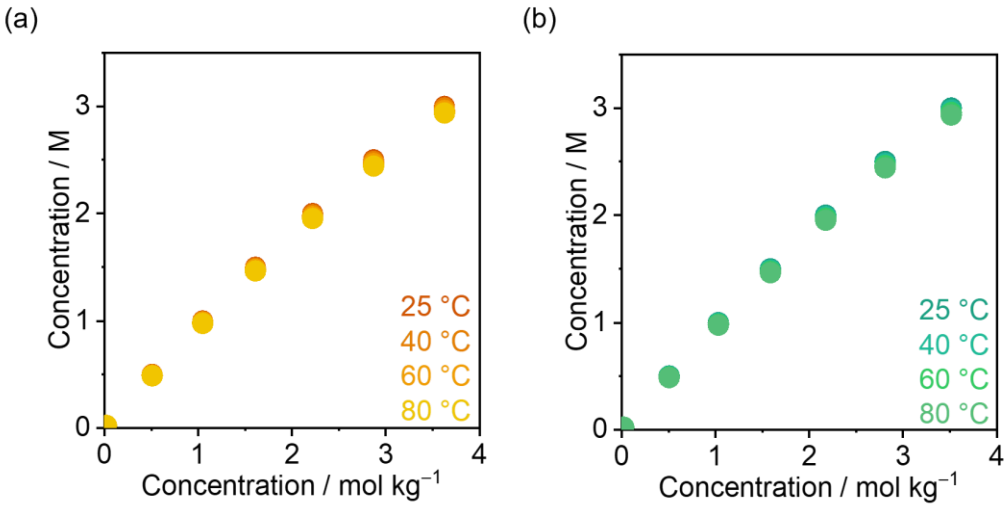

Fig. S8 The molarity at different temperatures obtained by densities measured experimentally and the relationship between molarity and molality (m). (a) K-phosphate. (b) K-carbonate.

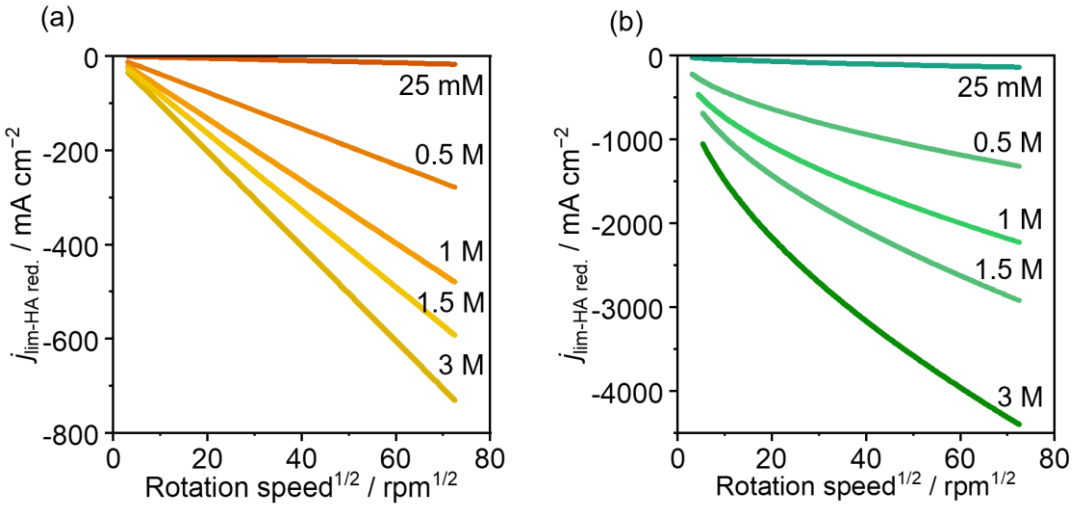

Fig. S9 (a) Levich plots of $j_{lim\text{-}HA\ red.}$ obtained from numerical simulations. Model with x M K-phosphate. (b) Model with x M K-carbonate. All of the electrolytes were assumed to have the same pH value as pK_a. A supporting electrolyte of 0.1 M $KClO_4$ was considered as an addition to the 25 mM buffer electrolytes. Pt rotating disk electrodes were assumed, and temperature is at 25 °C.

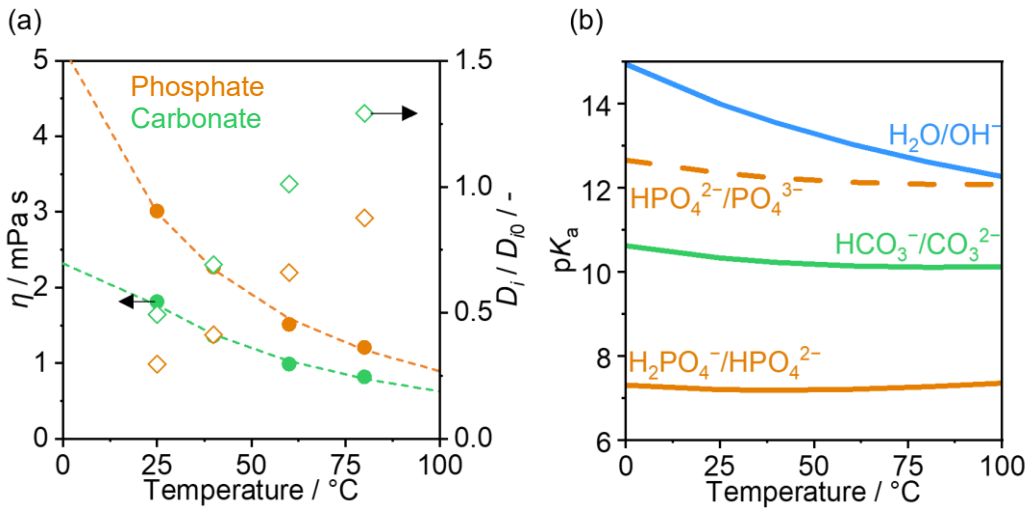

Fig. S10 (a) The relationships between temperature, viscosity and diffusion coefficients. Viscosities of 3 M K-carbonate solutions and 3 M K-phosphate were measured at different temperatures. Diffusion coefficients were corrected using the Stokes-Einstein relationship. (b) pK_a and pK_w as a function of temperature.

5. Temperature dependence

Equilibrium coefficients of homogeneous reactions

The pK_a and pK_w change according to temperature, following the next equation:[38]

$$\ln K' = \frac{\Delta H - T\Delta C_p}{R}\left(\frac{1}{T} - \frac{1}{T'}\right) + \frac{\Delta C_p}{R}\ln\left(\frac{T'}{T}\right) + \ln K \quad \text{(S6)}$$

where ΔH is enthalpy, ΔC_p is heat capacitance, and T' is goal temperature. This equation can be obtained when considering the change in enthalpy and entropy according to temperatures. The first term contributes to enthalpy change and the second term does to entropy change. The balance between these determines the temperature dependence of pK_a.

Table S1 Thermodynamic quantities for the ionization reactions of water and buffer ions[38]

	Equilibrium	pK_a at 25 °C	ΔH / kJ mol^{-1}	ΔC_p / J K^{-1} mol^{-1}
Water	K_w (H_2O/OH^-)	13.995	-	-
Carbonate	K_1 (H_2CO_3/HCO_3^-)	6.35	9.15	−371
	K_2 (HCO_3^-/CO_3^{2-})	10.33	14.70	−249
Phosphate	K_1 ($H_3PO_4/H_2PO_4^-$)	2.148	−8.0	−141
	K_2 ($H_2PO_4^-/HPO_4^{2-}$)	7.198	3.6	−230
	K_3 (HPO_4^{2-}/PO_4^{3-})	12.35	16.0	−242

Rate coefficients of homogeneous reactions

In this study, k_{af}, k_{bb} and k_{wf} were set as constants, and k_{ab}, k_{bf} and k_{wb} changed according to the equilibrium coefficients at different temperatures. This is because temperature dependence should follow the Arrhenius relationship with activation energy of the homogeneous reaction, which is difficult to measure. Here, the impact of this assumption was assessed. Fig. S11(a) and (b) show simulated $j_{\text{lim-HA red.}}$ in 3 M K-buffer solutions with pK_a 7 or 10 using different rate coefficients at 80 °C. While increasing rate coefficients did not affect $j_{\text{lim-HA red.}}$ in solution with pK_a 7, 10 times k_{bb} enhances $j_{\text{lim-HA red.}}$ in solution with pK_a 10. Fig. S11(c) expresses the deviation profile of equilibrium when k_{af}, k_{bb} and k_{wf} are not enhanced by temperature, indicating larger rate coefficients affect the ion distribution at closer than 1 μm. The decisive factor at small pK_a is diffusion of buffer species from

the bulk, which may not be affected. On the other hand, the enhancement in $j_{\text{lim-HA red.}}$ at large pK_a is caused by the acceleration of basic buffering action (Eq. 4). Thus, setting k_{bb} irrelevant to temperature can lead to underestimation of direct reduction of buffer species. Similarly for the OER, the acceleration of buffer protolysis (Eq. 3) is the cause of limiting current increase at small pK_a, indicating setting k_{af} constant can lead to underestimation.

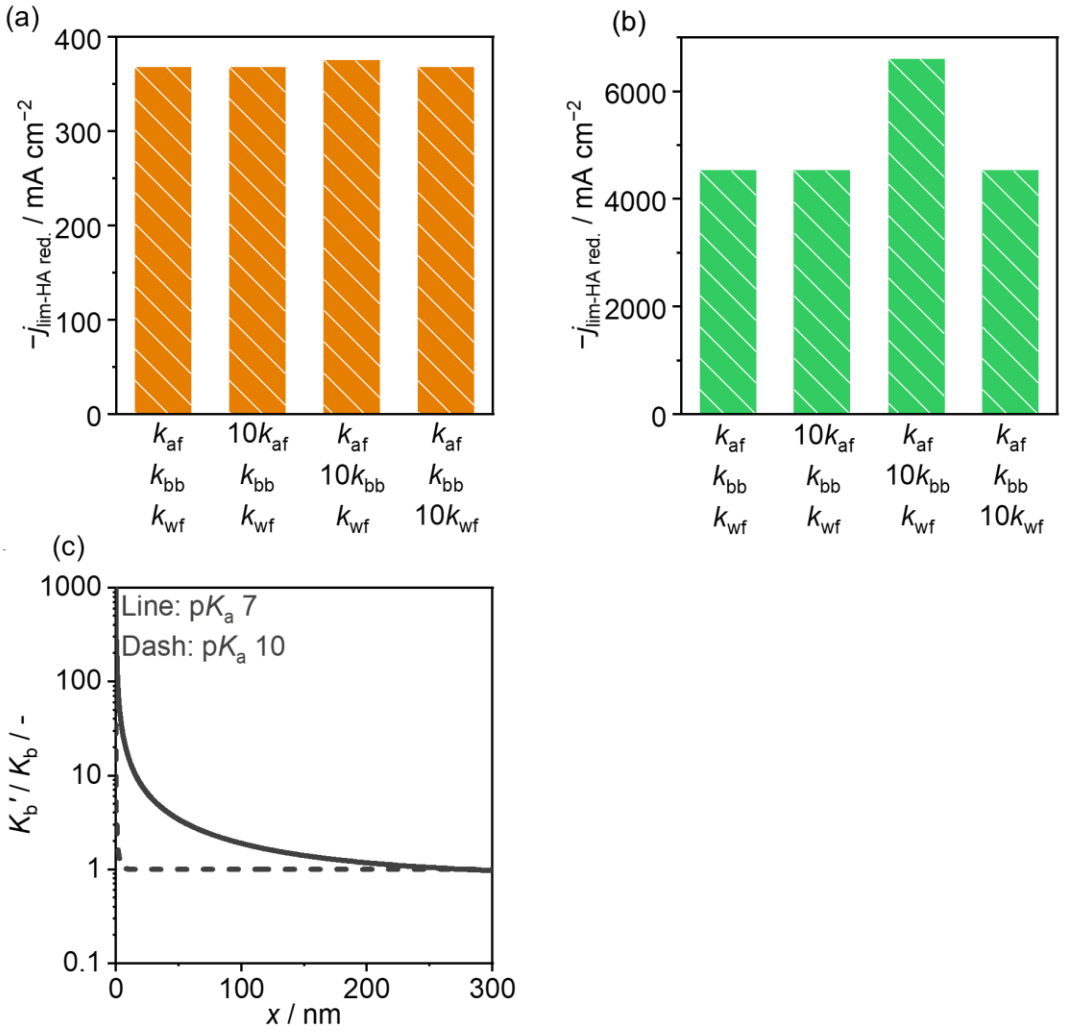

Fig. S11 (a) Calculated limiting current density of direct buffer reduction in 3 M $K_{1.5}H_{0.5}A$ solutions at pK_a = pH = 7 at 80 °C. The rate coefficients of homogeneous reactions were varied. The Pt rotating disk electrode was assumed to rotate at 100 rpm. (b) pK_a = pH = 10. (c) The deviation profile of equilibrium of basic buffering action (Reaction 4) when k_{af}, k_{bb} and k_{wf} are not enhanced by temperature. K_b' is the local value.

6. The limiting current density of direct buffer reduction

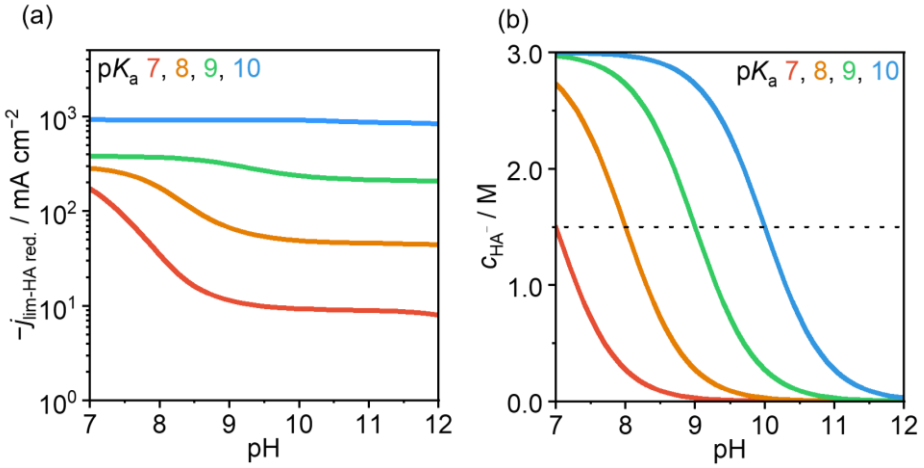

Fig. S12 (a) Calculated limiting current density of direct buffer reduction at different bulk pH at 25 °C. We assumed that the buffer was 3 M $K_{1.5}H_{0.5}A$ with pK_a ranging from 7–10. The total amount of buffer species was considered to be 3 M. The Pt rotating disk electrode was assumed to rotate at 100 rpm. Properties such as electrolyte viscosity, density, diffusion coefficients, and ion sizes were taken from 3 M K-carbonate solutions. (b) Relative ion fractions in bulk buffer solutions as a function of pH.

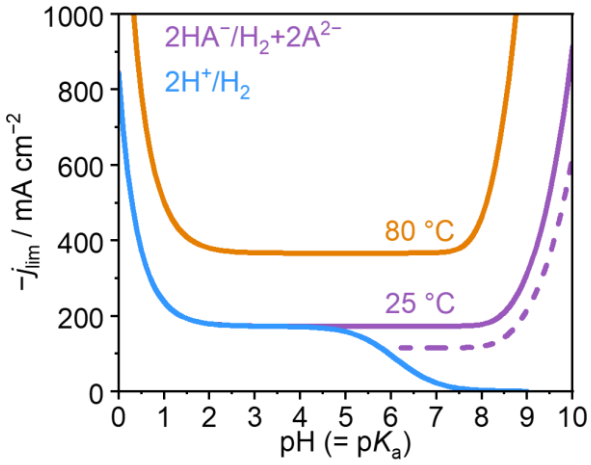

Fig. S13 The limiting current density of proton reduction (Reaction 1) and direct reduction of protonated buffer species (Reaction 5) during the HER in 3 M $K_{1.5}H_{0.5}A$ solutions. Electrolyte pH values were assumed to be the same as buffer's pK_a values. Pt RDE was assumed to rotate at 100 rpm. Properties such as electrolyte viscosity, density, diffusion coefficients, and ion sizes were taken from 3 M K-carbonate solutions.

7. Concentration profiles at limiting current of OER

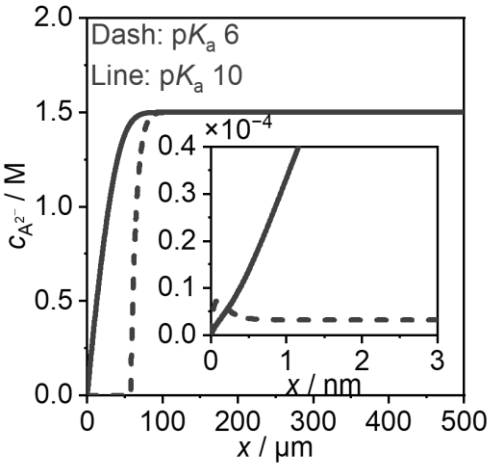

Fig. S14 Simulated concentration profile of deprotonated buffer species in the solutions as a function of distance from the electrode surface with the limiting current in 3 M $K_{1.5}H_{0.5}A$ solutions. Inset shows concentration profiles in the diffuse layer. Electrolyte pH values were assumed to be the same as buffer's pK_a values. Ni RDE was assumed to rotate at 100 rpm. Properties such as electrolyte viscosity, density, diffusion coefficients, and ion sizes were taken from 3 M K-carbonate solutions.

8. Charge dependence

The charge of buffer species also influences the limiting current density because the negatively charged cathode repels anions, while the positively charged anode attract anions. Fig. S15 shows the influence of the ion migration on $j_{\text{lim-HA red.}}$ and $j_{\text{lim-OH oxi.}}$. For simplicity, buffer ions were assumed to proceed a single-step buffer equilibrium (HA^x/A^{x-1}), and any other buffering equilibria were ignored. When looking at HER side, $-j_{\text{lim-HA red.}}$ shows decrease as charge of protonated buffer species goes negative. This result is consistent with previously reported experimental findings, in which positively charged hydrogen sources exhibited superior HER performance on Pt electrodes to phosphate buffer electrolytes.[49,50] On the other hand, the order of $j_{\text{lim-OH oxi.}}$ was $HA^+/A < HA^-/A^{2-} << HA/A^-$. It can be easily imagined that positively charged anodes attract negatively charged species. When both protonated buffer species and deprotonated buffer species are negatively charged, protonated buffer species can accumulate near the surface, which may inhibit deprotonated buffer species from coming to the surface. Thus, the combination of HA/A^- demonstrates the highest achievable current density. While optimizing the species charge is suggested by previous studies,[49,50] OER and HER are incompatible. Therefore, it is necessary to take different actions to enhance the mass transport.

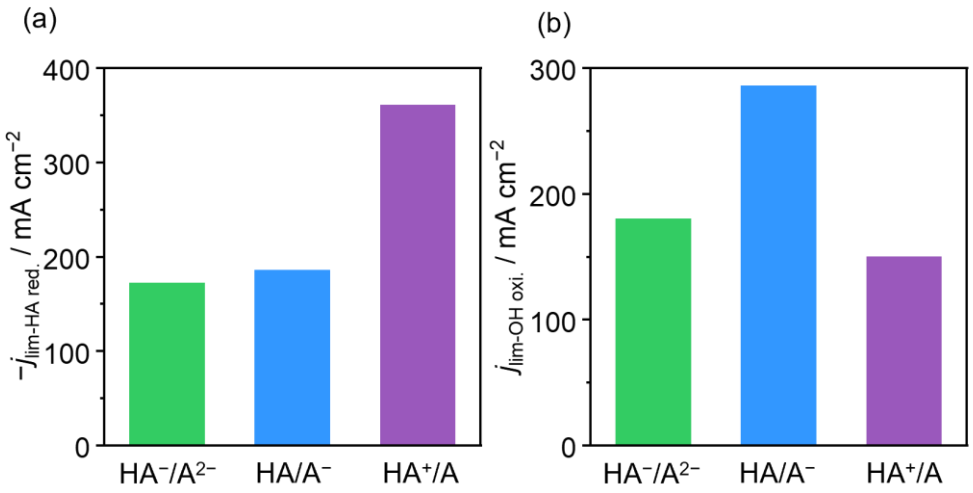

Fig. S15 (a) Dependence of $j_{\text{lim-HA red.}}$ on the charge of the proton source. Electrolytes were 3 M buffer solutions. Electrolyte was considered to be pH = pK_a = 7. Pt RDE was assumed to rotate at 100 rpm at 25 °C. (b) Dependence of $j_{\text{lim-OH oxi.}}$ on the charge of the deprotonated buffer species. Electrolytes were 3 M buffer solutions. Electrolyte was considered to be pH = pK_a = 10. Pt RDE was assumed to rotate at 100 rpm at 25 °C.

9. Rotation speed dependence

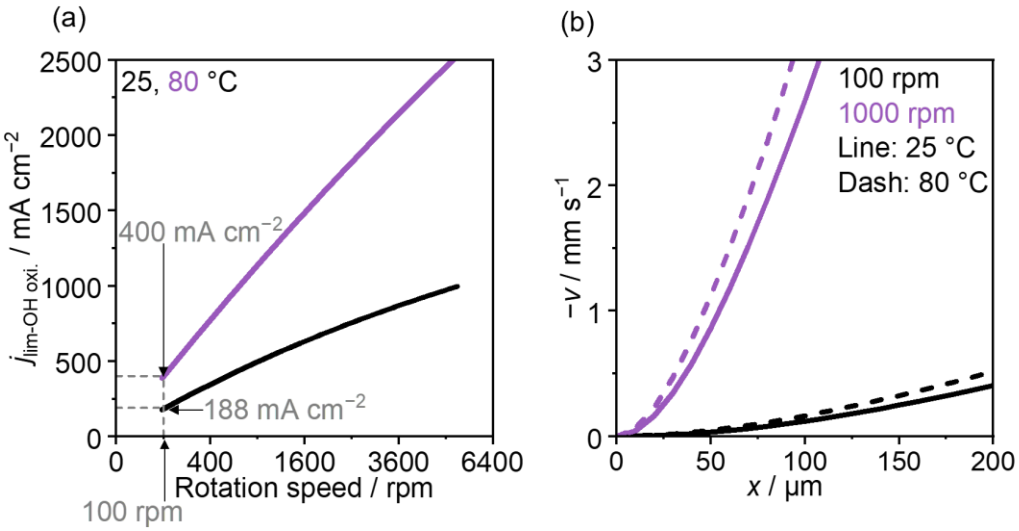

Fig. S16 (a) Dependence of $j_{\text{lim-OH oxi.}}$ on the rotation speed of the RDE. Electrolytes were 3 M $K_{1.5}H_{0.5}A$ solutions at pH = pK_a = 10. Properties such as electrolyte viscosity, density, diffusion coefficients, and ion sizes were taken from 3 M K-carbonate solutions. (b) The calculated fluid velocity on the RDE surface in 3 M K-carbonate electrolyte.

10. Parameters

Table S2 Ion size, A_i

i	Solvated sizes / m	References	Thermochemical sizes / m	References
H^+	0.56×10^{-9}	[55]	0.076×10^{-9}	[56]
OH^-	0.6×10^{-9}	[55]	0.266×10^{-9}	[57]
ClO_4^-	0.676×10^{-9}	[55]	0.48×10^{-9}	[57]
K^+	0.662×10^{-9}	[55]	0.276×10^{-9}	[56]
H_2CO_3	0.23×10^{-9}	[33]	0.23×10^{-9}	[33]
HCO_3^-	0.8×10^{-9}	[33]	0.312×10^{-9}	[57]
CO_3^{2-}	0.788×10^{-9}	[55]	0.356×10^{-9}	[57]
H_3PO_4	0.8×10^{-9}	Estimated	0.401×10^{-9}	Estimated
$H_2PO_4^-$	0.8×10^{-9}	Estimated	0.426×10^{-9}	[58]
HPO_4^{2-}	0.8×10^{-9}	Estimated	0.451×10^{-9}	Estimated
PO_4^{3-}	0.8×10^{-9}	Estimated	0.476×10^{-9}	[57]

Table S3 Homogeneous reactions

Constant	Value	Unit	Description	Reference
K_w	1×10^{-14}	mol L^{-1}		
k_{wf}	1.38×10^{-3}	s^{-1}		21
k_{wb}	1.38×10^{11}	L mol^{-1} s^{-1}	k_{wf}/K_w	
K_{ac1}	$1\times10^{-6.33}$	mol L^{-1}		38
K_{bc1}	$1\times10^{7.67}$	-	K_{ac1}/K_w	
K_{ac2}	$1\times10^{-10.3}$	mol L^{-1}		38
K_{bc2}	$1\times10^{3.7}$	-	K_{ac2}/K_w	
k_{afc1}	0.037	s^{-1}		40
k_{abc1}	8.2833×10^{4}	L mol^{-1} s^{-1}	k_{afc1}/K_{ac1}	
k_{bfc1}	2.23×10^{3}	L mol^{-1} s^{-1}		33,39
k_{bbc1}	5.0502×10^{-5}	L mol^{-1} s^{-1}	k_{bfc1}/K_{bc1}	
k_{afc2}	59.4	s^{-1}		40
k_{abc2}	1.185×10^{12}	L mol^{-1} s^{-1}	k_{afc2}/K_{ac2}	
k_{bfc2}	6×10^{9}	L mol^{-1} s^{-1}		33,39
k_{bbc2}	1.2976×10^{6}	L mol^{-1} s^{-1}	k_{bfc2}/K_{bc2}	
K_{ap1}	$1\times10^{-2.148}$	mol L^{-1}		38
K_{bp1}	$1\times10^{11.852}$	-	K_{ap1}/K_w	
K_{ap2}	$1\times10^{-7.198}$	mol L^{-1}		38
K_{bp2}	$1\times10^{6.802}$	-	K_{ap2}/K_w	
K_{ap3}	$1\times10^{-12.35}$	mol L^{-1}		38

K_{bp3}	$1\times10^{1.65}$	-	K_{ap3}/K_w	
k_{afp1}	7.4727×10^{8}	s^{-1}		21
k_{abp1}	1.0507×10^{11}	L mol^{-1} s^{-1}	k_{afp1}/K_{ap1}	
k_{bfp1}	5.3654×10^{7}	L mol^{-1} s^{-1}	$k_{bbp1}\times K_{bp1}$	
k_{bbp1}	7.54397×10^{-5}	L mol^{-1} s^{-1}		14
k_{afp2}	7.4814×10^{3}	s^{-1}		21
k_{abp2}	1.1803×10^{11}	L mol^{-1} s^{-1}	k_{afp2}/K_{ap2}	
k_{bfp2}	5.4903×10^{8}	L mol^{-1} s^{-1}	$k_{bbp2}\times K_{bp2}$	
k_{bbp2}	86.616	L mol^{-1} s^{-1}		14
k_{afp3}	5.9361×10^{-2}	s^{-1}		21
k_{abp3}	1.3289×10^{11}	L mol^{-1} s^{-1}	k_{afp3}/K_{ap3}	
k_{bfp3}	5.8884×10^{9}	L mol^{-1} s^{-1}	$k_{bbp3}\times K_{bp3}$	
k_{bbp3}	1.3183×10^{8}	L mol^{-1} s^{-1}		14

Table S4 Diffusion coefficient, D_{i0}, ($\mu_0 = 8.93\times10^{-4}$ Pa s)

i (D_{i0})	Value / $m^2\ s^{-1}$	Reference
H^+	9.311×10^{-9}	[38]
OH^-	5.273×10^{-9}	[38]
ClO_4^-	1.792×10^{-9}	[38]
K^+	1.957×10^{-9}	[38]
H_2CO_3	1.91×10^{-9}	[33]
HCO_3^-	1.185×10^{-9}	[38]
CO_3^{2-}	0.923×10^{-9}	[38]
H_3PO_4	0.959×10^{-9}	Estimated
$H_2PO_4^-$	0.959×10^{-9}	[38]
HPO_4^{2-}	0.759×10^{-9}	[38]
PO_4^{3-}	0.824×10^{-9}	[38]

Table S5 Potential related parameters

Constant	Value	Unit	Reference
ε_0	8.854×10^{-12}	F m^{-1}	[38]
ε_r	80.1	-	
C_{Stern}	20	μF cm^{-2}	[37]
PZC	0.23	V vs. SHE	[43]

Table S6 Input bulk concentration of species, $c_{i,\,Bulk}$ in 3 M K-buffer solutions at pH = pK_a = 7

i	Value / mol L^{-1}
H^+	1.00×10^{-7}
OH^-	1.01×10^{-7}
K^+	4.50
HA^-	1.50
A^{2-}	1.50
H_2O	1*

* We did not calculate the mass transport of water molecules, thus the concentration of water is set to 1 mol L^{-1} throughout the domain.